4 July 1997

ELSEVIER

Chemical Physics Letters 272 (1997) 383–390

CHEMICAL
PHYSICS
LETTERS

Kinetics of the gas phase reaction OH + NO(+ M) → HONO(+ M) and the determination of the UV absorption cross sections of HONO

Palle Pagsberg [a], Erling Bjergbakke [a], Emil Ratajczak [b], Alfred Sillesen [a]

[a] *Chemical Reactivity Section, Plant Biology and Biogeochemistry Department, Risø National Laboratory, DK-4000 Roskilde, Denmark*
[b] *Department of Physical Chemistry, Wroclaw University of Medicine, Pl. Nankiera 1, 50-140 Wroclaw, Poland*

Received 8 April 1997; in final form 28 April 1997

Abstract

The reaction OH + NO(+ M) → HONO(+ M) with M = SF_6 as a third body has been employed as a clean source for recording the near-ultraviolet absorption spectrum of HONO without interference from other absorbing species. The reaction was initiated by the pulse radiolysis of $SF_6/H_2O/NO$ mixtures with total pressures in the range 10–1000 mbar at 298 K. The pressure dependence of the rate coefficient was studied by time-resolved UV and IR spectroscopy. By analysis of the fall-off curve we have derived a value for the limiting low pressure rate constant $k_0/[SF_6] = (1.5 \pm 0.1) \times 10^{-30}$ cm^6 $molecule^{-2}$ s^{-1} at 298 K, using the values of $k_\infty = (3.3 \pm 0.3) \times 10^{-11}$ cm^3 $molecule^{-1}$ s^{-1} and $F_{cent} = 0.81$ reported by Troe and co-workers. The UV spectrum of HONO was recorded in the range 320–400 nm and an absolute absorption cross section of $\sigma = (5.02 \pm 0.76) \times 10^{-19}$ cm^2 $molecule^{-1}$ has been determined for the strongest band of HONO located at 354.2 nm. Differential absorption cross sections to be used for field measurements of HONO were also investigated. © 1997 Elsevier Science B.V.

1. Introduction

Nitrous acid plays an important role as a major source of OH radicals in polluted urban areas where direct emission from automobile exhaust has been unequivocally demonstrated [1]. During the day nitrous acid is decomposed by the reaction HONO + $h\nu \rightarrow$ OH + NO which proceeds with a near-unity quantum yield at 368 nm [2,3]. Long-path differential optical absorption spectroscopy (DOAS) has been developed for measurements of ambient concentrations of HONO which has a characteristic vibronic structure in the range 300–400 nm. The near-ultraviolet spectrum of HONO has been investigated in several laboratories using different source reactions for the formation of HONO [3–7]. while there is a general agreement about the vibronic structure, the determination of absolute absorption cross sections has been a difficult task because of the photolysis and thermal decomposition of HONO giving rise to reaction products absorbing in the same spectral region, i.e. NO_2, N_2O_4 and N_2O_3. The determination of absolute concentrations of HONO has been the main problem causing a wide scatter in the published absorption cross sections which differ by as much as a factor of 4.

PII S0009-2614(97)00576-9

In the present investigation we have employed the pulse radiolysis of $SF_6/H_2O/NO$ mixtures to initiate the following reactions:

$$F + H_2O \rightarrow HF + OH, \tag{1}$$

$$OH + NO(+M) \rightarrow HONO + (+M), \tag{2}$$

$$F + NO(+M) \rightarrow FNO(+M), \tag{3}$$

$$OH + OH(+M) \rightarrow H_2O_2(+M). \tag{4}$$

Reaction (2) provides a clean source of nitrous acid without interference from other absorbing species in the spectral range of interest. Ultraviolet absorption spectra were recorded on a timescale of 20–100 μs which is short compared with the time constant for the slow surface catalyzed decomposition of HONO towards the equilibrium $2\ HONO \rightleftharpoons NO + NO_2 + H_2O$. In order to determine the absolute concentration of HONO produced in reaction (2) we have employed the material balance defined in equation (I) including the initial yield of F atoms produced by the radiolysis of SF_6 as well as the unavoidable loss reactions (3) and (4).

$$[HONO] = [F]_0 - [FNO] - 2[H_2O_2]. \tag{I}$$

The initial yield of F atoms was determined using the titration reaction $F + CH_4 \rightarrow HF + CH_3$ and monitoring the transient absorption signals of CH_3 at 216.36 nm using a recommended value of the absorption cross section of $\sigma(CH_3) = (4.12 \pm 0.11) \times 10^{-7}$ cm^2 molecule^{-1} [8,9]. For comparison we have also monitored the yield of FNO produced in reaction (3) and the consumption of NO_2 in the reaction $F + NO_2 + M \rightarrow FNO_2 + M$ using recommended values of $\sigma(FNO)$ [10] and $\sigma(NO_2)$ [11]. Previously we studied the kinetics of reaction (3) and determined a value of $k_3 = (1.71 \pm 0.10) \times 10^{-11}$ cm^3 molecule^{-1} s^{-1} with $p(SF_6) = 1$ atm [12].

In the present investigation we have studied the kinetics and relative yields of OH, FNO and HONO, and the rate constants determined for the reactions (1)-(4) were employed in computer modeling to determine the relative yield of HONO in accordance with Eq. (I) as well as the absorption cross section of HONO at 354.2 nm. Previously [13–24], the pressure dependent rate coefficient of reaction (2) was studied by monitoring the OH decay kinetics at varying temperatures and pressures and with different third bodies, M = He, Ar, N_2, CF_4, H_2O and SF_6. In the present investigation we studied the formation kinetics of HONO employing UV spectroscopy at higher pressures and infrared diode laser spectroscopy at lower pressures to establish the major part of the fall-off curve for reaction (2) with $M = SF_6$ as the third body at total pressures in the range 10–1000 mbar at 298 K.

2. Experimental

The experimental apparatus for pulse radiolysis combined with transient UV absorption spectroscopy has previously been described in detail [25], and more recently we have employed infrared diode laser spectroscopy for the detection of short-lived radicals as well as stable product molecules [26]. In the present investigation the kinetics of OH and FNO were studied by monitoring the transient absorption signals at 309.04 and 311.2 nm, respectively. The UV spectrum of HONO was recorded in the range 320–400 nm, and the kinetics of reaction (2) were studied by monitoring the formation of HONO at 354.2 nm at pressures in the range 350–1000 mbar SF_6. However, in order to improve the performance at lower pressures we have employed infrared diode laser spectroscopy using a strong rotational transition within the ν_3 band at 1263.2069 cm^{-1} [27].

3. Experimental results and interpretation

3.1. Kinetics of HONO formation

Reaction (2) was initiated by the pulse radiolysis of $SF_6/H_2O/NO$ mixtures and an example of the observed formation kinetics at 354.2 nm is shown as an insert in Fig. 1. The kinetic curves were analysed using a simple pseudo-first order expression, $A(HONO) = A_{max}[1 - \exp(-k^* t)]$, where $k^* = k_0 + k_2[NO]_0$, and the rate constant was derived from the slope of the linear plot of k^* versus $p(NO)$. Similar experiments were carried out at lower bath gas pressures, and a summary is presented in Table 1. The yield of F atoms produced by the pulse radiolysis of SF_6 is nearly proportional to the total pressure of SF_6. Thus, due to the reduced yields obtained at total pressures below 350 mbar the for-

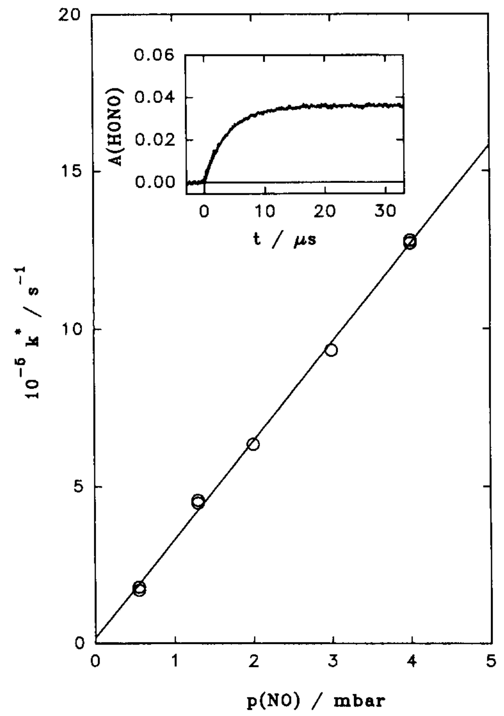

Fig. 1. Kinetics of the HONO formation monitored at 354.2 nm with an optical path length of 120 cm. A value of $k_2 = 1.30 \times 10^{-11}$ $cm^3 molecule^{-1} s^{-1}$ was obtained from the slope of k^* versus p(NO). The insert shows the rate of formation observed with partial pressures of $p(NO) = 0.5$ mbar and $p(H_2O) = 15$ mbar backed up with SF_6 to a total pressure of 1 atm at 298 K.

mation kinetics of HONO could not be monitored at 354.2 nm with a reasonable signal-to-noise ratio. To overcome these difficulties we have employed infrared diode laser spectroscopy for the detection of HONO at total pressures in the range 10–350 mbar. The ν_3 band of trans-HONO has previously been studied by Fourier transform spectroscopy with a spectral resolution of 0.05 cm^{-1} [28] and by tunable infrared diode laser spectroscopy [27]. Recently, absolute line strength measurements have been carried out in the range 1254.2–1255.2 cm^{-1} [29]. Unfortunately, the strong lines in this region could not be utilized in the present investigation because of overlap with the $\nu_2 + \nu_4$ band of SF_6 at 1255 cm^{-1} [30]. To avoid this overlap we have selected a fairly strong line of trans-HONO at 1240.339 cm^{-1} for kinetic studies. The same procedure was applied for the kinetic analysis of IR-transients, and the results obtained with total pressures of 10–350 mbar are also included in Table 1. The observed second-order rate constants for reaction (2) are strongly dependent on the total pressure in the range 10–1000 mbar. The kinetics of reaction (2) have been studied at high pressures with a maximum of $[M] = [He] = 3.2 \times 10^{21}$ $molecule\,cm^{-3}$ at 298 K [24]. Fig. 2 shows the fall-off curve for reaction (2) obtained in the present investigation in comparison with the results of previous studies with $M = SF_6$ [17,22]. Our experimental

Table 1

Experimental conditions and results on the pressure-dependent addition reaction $OH + NO(+M) \rightarrow HONO(+M)$ (2) with $M = SF_6$ at 298 K. Detection of HONO formation kinetics at 354.2 nm (UV) and at 1242 cm^{-1} (IR)

$p(SF_6)$ (mbar)	p(NO) (mbar)	$10^{-4}k^*$ (s^{-1})	No. of exp.	$10^{13}k_2$ (cm^3 $molecule^{-1}$ s^{-1})	Notes
10	0.12–0.45	0.23–0.56	10	4.02	IR [a]
20	0.15–0.61	0.65–1.48	9	7.13	IR [a]
40	0.15–0.60	1.56–2.84	10	12.9	IR [a]
60	0.20–0.61	2.78–5.21	9	21.6	IR [a]
100	0.10–0.61	3.47–7.07	12	29.4	IR [a]
200	0.28–2.05	5.57–24.0	23	46.5	IR [b]
350	0.30–2.30	5.20–37.1	10	65.4	UV,IR [b]
500	0.85–4.10	16.7–82.5	6	82.9	UV [b]
750	0.50–4.00	14.7–107	8	111	UV [a]
1000	0.55–4.00	18.0–127	8	130	UV [a]

[a] Estimated uncertainties of k are in the range 5–10%.

[b] Estimated uncertainties of k are in the range 10–15%.

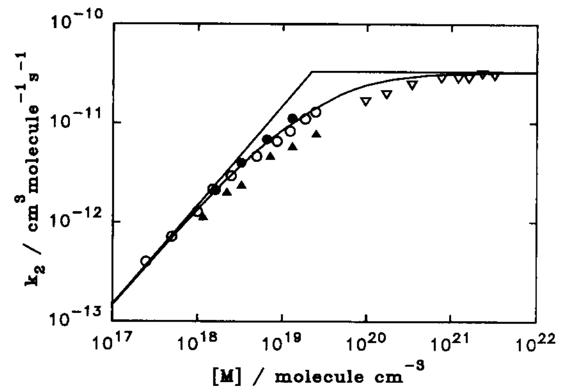

Fig. 2. Experimental fall-off curve for the reaction HO+NO(+M)→HONO(+M) with M = SF_6 at 298 K (hollow circles: this work, filled circles [22], filled triangles: [17], hollow triangles: [24] with M = He) and limiting high- and low-pressure rate constants.

results are in good agreement with the results obtained by studies of OH decay kinetics using laser-induced fluorescence in the range 66–526 mbar at 298 K [22]. Previous results based on OH kinetics monitored by resonance absorption are almost a factor of two lower in the range $p(SF_6) = 47-1014$ mbar at 295 K [17]. In the present investigation we have also studied reaction (2) by monitoring the OH decay kinetics at 309.04 nm. In the presence of NO we observed simple first order kinetics, $[OH] = [OH]_0 \exp(-k^* t)$, and the value of $k_2 = 1.27 \times 10^{-11}$ cm^3 molecule^{-1} s^{-1} obtained with 1000 mbar SF_6 at 298 K is close to the value obtained from HONO formation kinetics. In our analysis of the fall-off curve we have employed the following expression as recommended by Troe et al. [24]:

$$k_2 = \left[\frac{k_{2,0}}{1 + k_{2,0}/k_{2,\infty}}\right] \times F_{\text{cent}}^{(1 + (\log(k_{2,0}/k_{2,\infty})/0.75 - 1.27 \log F_{\text{cent}})^2)^{-1}} .$$

The best fit of our experimental results, represented by the solid line in Fig. 2, was obtained with a low pressure limiting rate constant of $k_{2,0}[SF_6] = 1.5 \times 10^{-30}$ cm^6 molecule^{-2} s^{-1} combined with values of $k_{2,\infty} = 3.3 \times 10^{-11}$ cm^3 molecule^{-1} s^{-1} and $F_{2,\text{cent}} = 0.81$ reported by Troe et al. [24]. Values of $k_{2,\infty}$ reported in previous evaluations are in the range $(1.0-3.2) \times 10^{-11}$ cm^3 molecule^{-1} s^{-1} [31]. However, the lower values were estimated based on limited parts of the fall-off curve near the low pressure limit.

3.2. UV-absorption cross sections of HONO

Fig. 3 shows the absorption spectrum of HONO produced by the pulse radiolysis of a gas mixture containing 2 mbar NO and 5 mbar H_2O backed up with SF_6 to a total pressure of 1 atm. The spectrum was recorded with an optical multichannel analyzer and a path length of 120 cm. In order to cover the spectral range 320–400 nm we have employed a grating with 150 lines/mm and an entrance slit width of 0.01 mm corresponding to a band pass of 0.06 rim. Under these conditions the spectral resolution is determined by the size of individual diodes in the array. A PEN-RAY neon lamp was used for wavelength calibration and determination. of a spectral resolution of 0.167 nm/diode. The calculated positions of the two most prominent bands at 354.3 and 368.2 nm are in good agreement with the results of previous studies. The spectrum shown in Fig. 3 corresponds to the amount of HONO produced by irradiation of the gas mixture with a single pulse of 2 MeV electrons. To improve the signal-to-noise ratio we have accumulated a total of 500 spectra before and after electron beam irradiation. At wavelengths below 340 nm the spectrum is contaminated with a minor contribution from FNO produced in reaction (3) taking place in competition with the OH source reaction (1). In order to determine reliable values of

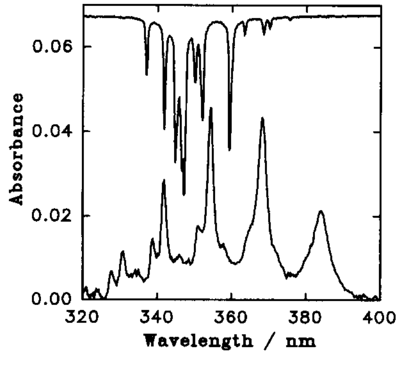

Fig. 3. UV spectrum of HONO recorded with an optical multichannel analyzer. Position of the most prominent band maxima at 341.8, 354.2, 368.2 and 384.1 nm were determined by wavelength calibration based on the neon lines shown above.

Table 2
Yield of F atoms produced by the pulse radiolysis of 1 atm SF_6 at 298 K

Species	λ (nm)	σ (cm^2 $molecule^{-1}$)	Ref.	$[F]_0$ (molecules cm^{-3})
CH_3	216.4	4.12×10^{-17}	[8,9]	2.62×10^{15}
FNO	311.2	6.10×10^{-19}	[10]	2.67×10^{15}
NO_2	444.8	7.25×10^{-19}	[11]	2.78×10^{15}

the absorption cross sections of HONO in the range 320–400 nm we have carried out detailed computer simulations of the chemical reaction mechanism including unavoidable loss reactions, where reaction (3) dominates at high NO concentrations while the fast self-reaction (4) becomes increasingly important at low NO concentrations. The kinetics of OH in the absence of NO were studied by monitoring the transient absorption at 309.04 nm. The rate of formation was studied at varying H_2O concentrations to derive a value of $k_1 = 2.0 \times 10^{-11}$ cm^3 $molecule^{-1}$ s^{-1}.

The decay of OH was studied using partial pressures of $p(H_2O) > 5$ mbar to ensure that all F atoms were consumed in reaction (1). A value of $k_4 = 1.3 \times 10^{-11}$ cm^3 $molecule^{-1}$ s^{-1} at 1 atm of SF_6 was derived by computer modeling of the experimental curves using the yield of F atoms listed in Table 2. The primary yield of F atoms was determined by a comparison of results obtained with three different titration reactions initiated by the pulse radiolysis of SF_6 in the presence of CH_4, NO or NO_2. The yields of CH_3 and FNO were determined by monitoring the maximum absorptions at 216.4 and 311.2 nm, respectively, while the consumption of NO_2 was monitored at 444.8 nm. Table 2 shows a summary of the yields of F atoms determined by the three different titration reactions. In the case of NO_2 we have employed a value for the absorption cross section corresponding to a spectral resolution of 0.1 nm.

The yield of HONO obtained with varying $[NO]/[H_2O]$ concentration ratios was studied by monitoring the formation kinetics at the absorption maximum at 354.2 nm. As shown in Fig. 4 the yield goes through a maximum, and the decrease at higher NO concentrations is due to the loss of F atoms via reaction (3). Previously, we studied the pressure dependence of this reaction and determined a value of $k_3 = 7.5 \times 10^{-12}$ cm^3 $molecule^{-1}$ s^{-1} with 1 atm SF_6 at 298 K [12]. The competition between reactions (1) and (3) was also studied directly by monitoring the formation kinetics of FNO at 311.2 nm. The yield of FNO was found to decrease to 50% of the maximum value when water vapor was added to a concentration ratio of $[H_2O]/[NO] = k_3/k_1 = 0.375$. Considering the competition between reactions (1) and (3) the loss of F atoms via reaction (3) can be reduced to a small fraction by the use of the highest possible concentration of water. However, experimental results obtained with $p(H_2O) > 15$ mbar at 298 K were not considered to be reliable because of aerosol formation which interferes with the optical absorption measurement. At lower partial. pressures, i.e. $p(H_2O) < 10$ mbar we did not observe any aerosol formation. In order to obtain the most reliable measurements of the water concentration we have chosen to work with partial pressures in the range 0–5 mbar. The experimental yields of HONO shown in Fig. 4 were obtained with $p(H_2O) = 3$ mbar. The yield curve was analysed by detailed computer modeling of the complete reaction mechanism involving the reactions (1)–(4) as well as the reaction $OH + HONO \rightarrow H_2O + NO_2$ which was shown to be important only at low NO concentrations. The yield of HONO was found to go through a maximum corresponding to $[HONO]_{max}/[F] = 0.80 \pm 0.05$ where the estimated uncertainty is based on a

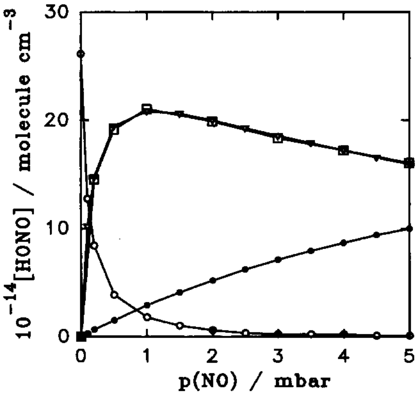

Fig. 4. Experimental yields of HONO monitored at 354.2 nm (squares). The yield curve was reproduced by computer modeling (triangle) of the reaction mechanism employing a scaling factor $A = \sigma L[HONO]$ using $\sigma(HONO) = 5.02 \times 10^{-19}$ cm^2 $molecule^{-1}$. The relative yields of H_2O_2 (open circles) and FNO (filled circles) obtained by modeling are also included.

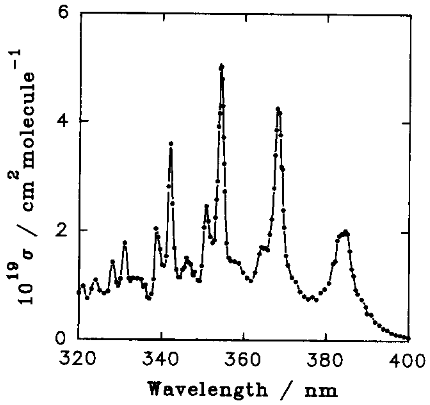

Fig. 5. UV spectrum of HONO obtained by 150 single-pulse experiments where the formation kinetics of HONO were monitored at selected wavelengths with an optical path length of 120 cm and a spectral band pass of 0.4 nm. Virtually no effect of spectral resolution was observed by comparison of the shape and maximum of the band at 354.2 nm with band passes of 0.4 and 0.25 nm, respectively.

sensitivity analysis with respect to the rate constants employed in the computer simulations of the reaction mechanism. The experimental curve was reproduced by the model using the following value of the absorption cross section, $\sigma(\mathrm{HONO}) = 5.02 \times 10^{-19}$ cm^2 molecule^{-1} at 354.2 nm. This value is close to the value of 4.96×10^{-19} cm^2 molecule^{-1} reported by Stockwell and Calvert [6] and about 20% lower than the value reported by Bongartz et al. [7] which has been recommended in the most recent data evaluation by NASA in 1994. In order to determine reliable differential absorption cross sections for DOAS we have recorded the most prominent features of the HONO spectrum in the range 320–400 nm. The spectrum shown in Fig. 5 is the result of 150 single-pulse experiments where the formation kinetics of HONO at the selected wavelength were monitored on a timescale of 200 μs.

At wavelengths below 350 nm the spectrum has been corrected for minor contributions from FNO produced in reaction (3). The spectral range 345–380 nm is of particular interest for field measurements of HONO by DOAS. In order to provide the most reliable absorption cross sections for this region we have employed curve fitting of an analytical expression based on a sum of Lorentzian lineshapes,

$$\sigma(\mathrm{HONO}) = \Sigma A_i / \left(1 + \left((\lambda - \lambda_i)/B_i\right)^2\right).$$

After adjustments of the amplitudes, A_i, and broadening factors, B_i, at different band centers, λ_i, shown in Table 3 we have been able to reproduce the experimental spectrum within the signal-to-noise ratio. The absolute absorption cross sections listed in Tables 4 and 5 have been used to evaluate differential absorption cross sections for the bands at 354.2 and 368.2 nm. Based on adjacent maxima and minima we have obtained the following values of $\Delta\sigma(354.2/352.2) = 3.24 \times 10^{-19}$ cm^2 molecule^{-1} and $\Delta\sigma(354.2/357.0) = 3.62 \times 10^{-19}$ cm^2 molecule^{-1} which may be compared with the values of 4.94×10^{-9} and 5.28×10^{-19} cm^2 molecule^{-1} published by Bongartz et al. [7]. Recently these values have been reevaluated and it was recommended that the published absorption cross sections should be multiplied by a factor of 0.855 [32].

The strong band of HONO at 254.2 nm nearly coincides with a NO_2 line of similar strength. Therefore, it has been suggested that the HONO band at 368.2 rim, where NO_2 interference is less severe, may be more useful for HONO detection by DOAS based on a differential absorption cross section of $\Delta\sigma(368\ \mathrm{nm}) = (2.34 \pm 0.01) \times 10^{-19}$ cm^2 molecule^{-1} [33].

From the absorption cross sections listed in Table 4 we have derived the following values of $\Delta\sigma(368.2/365.2) = 2.67 \times 10^{-19}$ cm^2 molecule^{-1} and $\Delta\sigma(368.2/372.2) = 3.27 \times 10^{-19}$ cm^2 molecule^{-1}. The average value of 2.67×10^{-19} cm^2 molecule^{-1} based on close-lying minima is 27% higher than the value reported by Febo et al. [33].

Table 3

Optimized parameters for the analytical expression $\sigma(\mathrm{HONO}) = \Sigma A_i/(1+((\lambda-\lambda_i)/B_i)^2)$

λ_i (nm)	A_i	B_i
346.0	0.0140	2.0
350.8	0.0190	1.1
354.2	0.0460	0.9
358.6	0.0105	2.6
364.2	0.0110	1.9
368.2	0.0410	1.3
373.0	0.0060	2.0
378.0	0.0030	1.5
383.3	0.0200	2.9

Table 4
Absorption cross sections of the 354.2 nm band of HONO

λ (nm)	$10^{19}\sigma$ (cm^2 $molecule^{-1}$)	λ (nm)	$10^{19}\sigma$ (cm^2 $molecule^{-1}$)	λ (nm)	$10^{19}\sigma$ (cm^2 $molecule^{-1}$)
348.0	1.11	354.0	4.82	358.0	1.46
348.4	1.08	354.2	5.02	358.2	1.47
348.8	1.11	354.4	4.81	358.4	1.47
349.2	1.23	354.6	4.30	358.6	1.47
349.6	1.44	354.8	3.68	358.8	1.46
350.0	1.80	355.0	3.10	359.0	1.44
350.4	2.23	355.2	2.63	359.2	1.41
350.8	2.47	355.4	2.26	359.4	1.38
351.2	2.32	355.6	1.99	359.6	1.34
351.6	2.01	355.8	1.79	359.8	1.30
352.0	1.81	356.0	1.64	360.0	1.26
352.2	1.78	356.2	1.54	360.2	1.22
352.4	1.81	356.4	1.47	360.4	1.18
352.6	1.91	356.6	1.43	360.6	1.15
352.8	2.07	356.8	1.41	360.8	1.13
353.0	2.32	357.0	1.40	361.0	1.11
353.2	2.66	357.2	1.40	361.2	1.10
353.4	3.12	357.4	1.41	361.4	1.10

The large discrepancies between published values of absolute and differential absorption cross sections of HONO must be ascribed to uncertainties in the determinations of absolute HONO concentrations. The experimental technique employed in the present investigation has allowed us to determine the absolute

Table 5
Absorption cross sections of the 368.2 nm band of HONO

λ (nm)	$10^{19}\sigma$ (cm^2 $molecule^{-1}$)	λ (nm)	$10^{19}\sigma$ (cm^2 $molecule^{-1}$)	λ (nm)	$10^{19}\sigma$ (cm^2 $molecule^{-1}$)
362.0	1.14	368.0	4.31	372.0	1.12
362.4	1.21	368.2	4.39	372.2	1.12
362.8	1.32	368.4	4.29	372.4	1.12
363.2	1.46	368.6	4.03	372.6	1.12
363.6	1.60	368.8	3.68	372.8	1.11
364.0	1.71	369.0	3.28	373.0	1.10
364.4	1.76	369.2	2.90	373.2	1.08
364.8	1.75	369.4	2.55	373.4	1.05
365.2	1.72	369.6	2.26	373.6	1.01
365.6	1.74	369.8	2.01	373.8	0.97
366.0	1.83	370.0	1.80	374.0	0.93
366.2	1.92	370.2	1.63	374.2	0.88
366.4	2.05	370.4	1.49	374.4	0.84
366.6	2.22	370.6	1.39	374.6	0.81
366.8	2.44	370.8	1.30	374.8	0.77
367.0	2.71	371.0	1.24	375.0	0.75
367.2	3.02	371.2	1.19	375.4	0.71
367.4	3.38	371.4	1.16	375.8	0.69
367.6	3.75	371.6	1.14	376.2	0.69
367.8	4.08	371.8	1.12	376.6	0.71

concentration of HONO with an estimated uncertainty of ±15%.

4. Conclusion

The fast reaction $OH + NO(+M) \rightarrow HONO(+M)$ has been employed as a clean source reaction for recording the near-ultraviolet absorption spectrum of HONO without interference from NO_2 and other absorbing NO_x species. The yield of HONO produced by the pulse radiolysis of $SF_6/H_2O/NO$ mixtures was determined by detailed computer simulations of the reaction mechanism taking into account unavoidable loss reactions producing H_2O_2 and FNO of which the latter contributes to the observed UV absorption at wavelengths below 350 rim. The absolute absorption cross sections of HONO listed in Tables 3 and 4 were derived by comparison with well established absorption cross sections of CH_3, FNO and NO_2 shown in Table 2. The estimated uncertainty of $\delta(\sigma(\mathrm{HONO})) = \pm 15\%$ is based on published uncertainties of the absorption cross sections of the reference compounds listed above and our determination of the relative yield of $[\mathrm{HONO}]_{\mathrm{max}} = (0.80 \pm 0.05)[\mathrm{F}]_0$. Thus, despite fairly large disagreements with previously published results we conclude that the absorption cross sections of HONO obtained in the present investigation may be taken with confidence.

Acknowledgements

These studies were carried out as a contribution to a research project 'Formation and Occurrence of Nitrous Acid in the Atmosphere' financed by the European Community. One of us (ER) gratefully acknowledges financial support from the Danish Natural Science and Research Council.

References

[1] J.N. Pitts Jr., H.W. Biermann, A.M. Winer, E.C. Tuazon, Atmos. Environ. 18 (1984) 847.
[2] R.A. Cox, J. Photochem. 3 (1974) 291.
[3] R.A. Cox, R.G. Derwent, J. Photochem. 6 (1976/77) 23.
[4] O.W. King, D. Moule, Can. J. Chem. 40 (1962) 2057.
[5] H.S. Johnston, R. Graham, Can. J. Chem. 52 (1974) 1415.
[6] W.R. Stockwell, J.O. Calvert, J. Photochem. 8 (1978) 193.
[7] A. Bongartz, J. Kames, F. Welter, U. Schurath, J. Phys. Chem. 95 (1991) 1076.
[8] H. Hippler, K. Luther, A.R. Ravishankara, J. Troe, Z. Phys. Chem. 142 (1984) 1.
[9] M.T. Mcpherson, M.J. Pilling, M.J.C. Smith, J. Phys. Chem. 89 (1985) 2268.
[10] J.D. Burley, C.E. Miller, H.S. Johnston, J. Mol. Spectrosc. 158 (1993) 377.
[11] W. Schneider, G.K. Moortgat, G.S. Tyndall, J.P. Burrows, J. Photochem. Photobiol. A: Chem. 40 (1987) 195.
[12] P. Pagsberg, A. Sillesen, J.T. Jodkowski, E. Ratajczak, Chem. Phys. Lett. 249 (1996) 358.
[13] F. Stuhl, H. Niki, J. Chem. Phys. 57 (1972) 3677.
[14] C. Morley, I.M. Smith, J. Chem. Soc. Faraday Trans. 68 (1972) 1016.
[15] A.A. Westenberg, N. DeHaas, J. Chem. Phys. 57 (1972) 5375.
[16] C.J. Howard, K.M. Evenson, J. Chem. Phys. 61 (1974) 1943.
[17] R. Overend, O. Paraskevopoulus, C. Black, J. Chem. Phys. 64 (1976) 4149.
[18] B.K.T. Sie, R. Simonaitis, J. Heicklen, Int. J. Chem. Kinet. 8 (1976) 99.
[19] C. Anastasi, I.W.M. Smith, J. Chem. Soc. Faraday Trans. 274 (1978) 1056.
[20] J.P. Borrows, T.J. Wallington, R.P. Wayne, J. Chem. Soc. Faraday Trans. 279 (1983) 111.
[21] E.R. Lovejoy, T.P. Murrells, A.R. Ravishankara, C.J. Howard, J. Phys. Chem. 94 (1990) 2386.
[22] S. Zabarnick, Chem. Phys. 171 (1993) 265.
[23] P. Sharkay, I.R. Sims, I.W.M. Smith, P. Bocherel, B.R. Rowe, J. Chem. Soc. Faraday Trans. 90 (1994) 3609.
[24] R. Forster, M. Frost, D. Fulle, H.F. Hamann, H. Hippler, A. Schlepegrell, J. Troe, J. Chem. Phys. 103 (1995) 2949.
[25] P. Pagsberg, O.J. Nielsen, C. Anastasi, in: Spectroscopy in Environmental Science, R.J.H. Clark, R.E. Hester (Eds.), John Wiley, Amsterdam, 1995, p. 263.
[26] P. Pagsberg, E. Ratajczak, A. Sillesen, in: Research in Chemical Kinetics, Vol. 1, R.G. Compton, G. Hancock (Eds. Elsevier, Amsterdam, 1993, p. 65.
[27] A.G. Maki, J. Mol. Spectrosc. 127 (1988) 104.
[28] C.M. Deeley, I.M. Mills, J. Mol. Struct. 100 (1983) 199.
[29] K.H. Becker, J. Kleffmann, R. Kurtenbach, P. Wiesen, Geophys. Res. Lett. 22 (1995) 2485.
[30] C. Chapados, G. Bimbaum, J. Mol. Spectrosc. 132 (1988) 232.
[31] R. Atkinson, D.L. Baulch, R.A. Cox, R.F. Hampson Jr., J.A. Kerr, J. Troe, J. Phys. Chem. Ref. Data 21 (1992) 1125.
[32] A. Bongartz, J. Kames, U. Schurath, C. George, P. Mirabel, J.L. Ponche, J. Atmos. Chem. 18 (1994) 149.
[33] A. Febo, C. Perrino, I. Allegrini, Atmos. Environ. 30 (1996) 3599.